Available online at www.sciencedirect.com
SCIENCE DIRECT®
Solid State Sciences 5 (2003) 35–45
Solid State Sciences
www.elsevier.com/locate/ssscie

Ab-initio construction of some crystalline 3D Euclidean networks

S.T. Hyde *, S. Ramsden, T. Di Matteo, J.J. Longdell

Applied Mathematics Dept., Research School of Physical Sciences, Australian National University, Canberra, ACT, 0200, Australia

Received 5 July 2002; accepted 10 September 2002

Dedicated to Sten Andersson for his scientific contribution to Solid State and Structural Chemistry

Abstract

We describe a technique for construction of 3D Euclidean (E^3) networks with partially-prescribed rings. The algorithm starts with 2D hyperbolic (H^2) tilings, whose symmetries are commensurate with the intrinsic 2D symmetries of triply periodic minimal surfaces (or infinite periodic minimal surfaces, IPMS). The 2D hyperbolic pattern is then projected from H^2 to E^3, forming 3D nets. Examples of cubic and tetragonal 3-connected nets with up to 288 vertices per unit cell, each linking a pair of 6-rings and a single 8-ring, are derived by projection onto the P, D, Gyroid and I-WP IPMS. A single example of a projection from close-packed trees in H^2 to E^3 (via the D surface) is also shown, that leads to a quartet of interwoven equivalent chiral nets. The configuration describes the channel system of a novel quadracontinuous branched minimal surface that is a chiral foam with four identical, open bubbles.

Keywords: Hyperbolic geometry; Crystalline graphs; Chemical frameworks

1. Introduction

Solid state chemistry is fertile ground for interesting geometrical challenges. Structural chemists, like Sten Andersson, have their way of finding the most reasonable answers. A good account of that approach can be found in his prescient 1983 "review", a manifesto on form in atomic systems, that still sparkles with imagination and insight [1]. Our offering here is somewhat duller and less intuitive. But it is, we think a useful *algorithmic* process to generate 3D crystalline nets. The process sidesteps the deep intuitive knowledge of 3D Euclidean space that Sten displays.

Recently, we were confronted with a structural challenge, that is easy to pose, but less easy to solve. The problem, that arose from analysis of a novel carbon material, is to construct "regular" three-connected nets containing only 6- and 8-rings. Some related examples are known already [2, 3], but to our knowledge the nets derived here are new (and not easy to derive from usual techniques). Their "regularity" requirement is set by the chemistry of C–C sp^2 bonding: the nets should have as far as practicable, equal edge lengths and vertex angles. Also, we expect non-bonded interatomic distances to exceed those of bonded atoms: nearest vertices should be linked by an edge. By analogy with the fullerene, C_{60}, we demand that each vertex lies on two 6-rings and a single 8-ring (vertex symbol (6.6.8), cf. (6.6.5) for C_{60}).

2. 2D non-Euclidean nets and crystallography

Our route to construction of suitable networks bypasses the intricacies of 3D Euclidean space until the very last step. Instead, we work in 2D hyperbolic space, or the hyperbolic plane, H^2. The reason is simple: 2D nets whose vertices are common to q p-rings are necessarily hyperbolic if

$$(p-2)(q-2) \succ 4. \tag{1}$$

In addition, truly *regular* examples of $\{p, q\}$[1] are possible in H^2 for all p, q satisfying Eq. (1). The hyperbolic plane has a wealth of regular tilings, far richer than Euclidean 2D (or 3D) space.

By analogy with conventional Euclidean crystallography, tilings in H^2 are described by symmetry groups known as *orbifolds*. The orbifold concept, due to Thurston (see [4]), is a very useful one, particularly for 2D groups, be they elliptic, flat or hyperbolic. (They allow for an almost

* Corresponding author.
E-mail address: stephen.hyde@anu.edu.au (S.T. Hyde).

[1] The first entry denotes the order of the (regular hyperbolic) polygon, the second the number of such polygons incident at vertices.

1293-2558/03/$ – see front matter
doi:10.1016/S1293-2558(02)00079-1

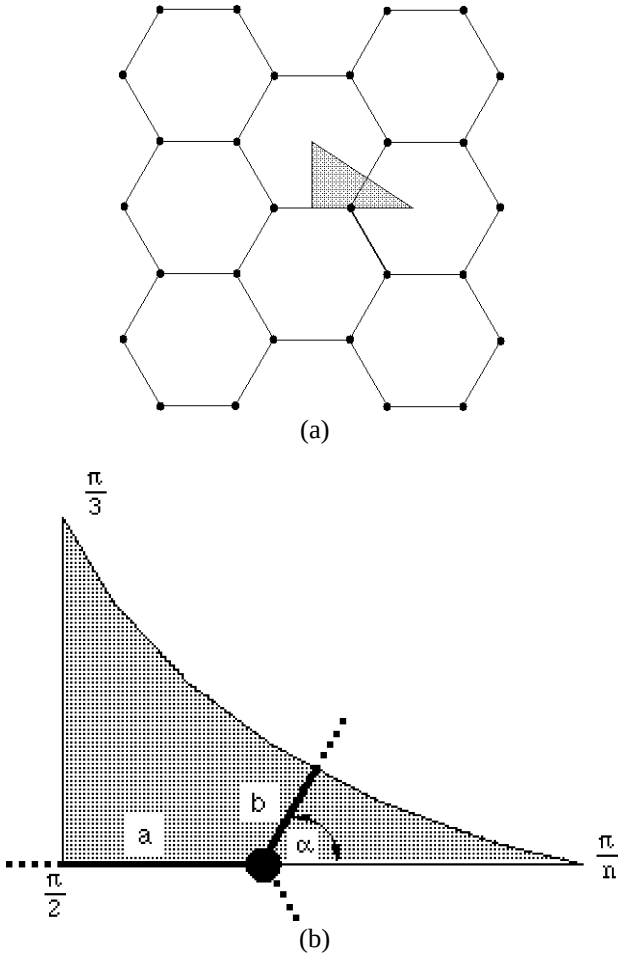

Fig. 1. (a) The {6,3} network (6.6.6), a Platonic tiling of the Euclidean plane, E^2. The hatched triangle denotes a domain of E^2 bounded by mirrors intersecting at $\pi/2, \pi/3$ and $\pi/6$, that covers E^2 by repeated reflections in those mirrors, forming the universal cover. The triangle defines a single ^{*236} orbifold. The {6,3} net can be produced by decoration of that domain with a (half) vertex and edges. (b) A single triangular $^*23n$ orbifold, whose universal cover is a (6.6.n) tiling.

trivial enumeration of planar (wallpaper) groups, as well as all point groups.) The orbifold symbol, invented by John Conway, is a character string whose entries define the symmetry in an extremely elegant fashion [5].

We need consider here only two of the four possible symmetry operations in 2D: reflection (in a line) and rotational symmetries. (Other possible operations—translations and glide reflections—are a product of these first two operations for all examples treated here.) The most symmetric patterns are those whose fundamental domains are bounded by intersecting reflection lines. Coxeter, naturally enough, called these *kaleidoscopic* groups [6]. These examples consist of a closed polygon, bounded by mirrors (lines). Denote the vertex angles of the polygon by $\pi/a, \pi/b, \pi/c \ldots$ The resulting orbifold symbol is $^*abc \ldots$ For example, a subset of the reflections in the regular graphite net, {6,3}, has orbifold symbol ^{*236} (Fig. 1a).

Table 1
Character strings and costs associated with 2D symmetry elements of orbifolds. The orbifold characteristic is calculated from these costs (Eq. (1)). The string nomenclature is applicable to any 2D symmetric pattern, whether it is elliptic, planar or hyperbolic. (Crystallographic point groups are elliptic, 2D planar groups are Euclidean.)

Symmetry element	Symbol	ζ_i
Mirror	*	1
Glide reflection	×	1
n-fold rotation center (cone point)	n	$\frac{n-1}{n}$
Mirror intersection (angle π/n)	n	$\frac{n-1}{2n}$
Translation	°	2

The symbol string allows direct reckoning of the cost of the orbifold, via the equation:

$$c = 2 - \sum_i \zeta_i, \tag{2}$$

where ζ_i values are associated with each character entry in the orbifold symbol (Table 1). Conway's notation is more than concise: the cost per orbifold is in fact identical to the Euler–Poincaré characteristic, and scales linearly with the integral Gaussian curvature of the asymmetric domain in the relevant 2D space. Since the spaces are of constant Gaussian curvature, the Gauss–Bonnet theorem implies that the cost also scales with the area of the asymmetric domain. If the cost is positive, the geometry is elliptic (e.g. spherical 2D groups, the crystallographic point groups); zero implies Euclidean character (usual 2D planar groups); negative costs are associated with hyperbolic space.

Decoration of the ^{*236} orbifold leads to the regular (6.6.6), or {6,3} net (Fig. 1a). Simple arithmetic confirms the Euclidean nature of this 2D pattern: the cost $(2 - (1 + 1/4 + 2/6 + 5/12))$ vanishes, and the integral curvature of the orbifold is zero. We generalize a little. We can "symmetry mutate" [7] the graphite net to give elliptic and hyperbolic analogs of graphite. Identical decoration of a $^*23n$ kaleidoscopic orbifold leads to the *semi*-regular (6.6.n) net, with two symmetrically distinct edges (Fig. 1b).

The ^{*235} pattern, with a positive cost (Euler–Poincaré characteristic $= 2 - (1 + 1/4 + 2/6 + 4/10) = 1/60$) gives the (6.6.5) net. The elliptic plane can be mapped into E^3 via projection onto the 2D sphere, S^2 (or any topologically identical closed shell), whose Euler–Poincaré characteristic is 2. To close the shell, 120 orbifold domains are needed, each with a half vertex, or 60 vertices *in toto*. This net is equivalent to C_{60} (and the ^{*235} orbifold is the Schoenflies point group I_h).

Recall that we seek the (6.6.8) net topology, which is realizable in H^2, via decoration of ^{*238} according to Fig. 1b. The resulting tiling is drawn in the Poincaré disc model of H^2 [8] in Fig. 2.

(H^2 is massively more superficial than the 2D disc. The Poincaré model manages to squeeze all of H^2 into the disc by extreme radial compression, without disrupting any angles. Indeed, the (6.6.8) net in Fig. 2 can be drawn with identical

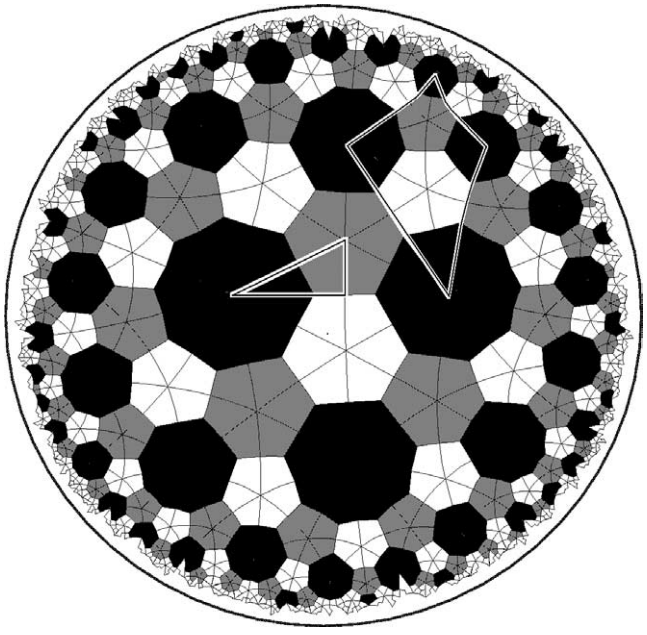

Fig. 2. The most symmetric form of the (6.6.8) network in the hyperbolic plane, H^2. Adjacent rings are shaded for convenience. Single copies of ^{*238} and ^{*2424} orbifolds are marked by the triangle and quadrilateral (cf. Fig. 1b). The Poincaré disc model of H^2 is used here, that allows the entire H^2 space to be mapped into a unit (2D Euclidean) disc. The map is conformal—angles are unchanged on mapping into the Poincaré disc—though lengths are increasingly foreshortened as the boundary of the disc is approached.

vertex angles of 120° everywhere. The edges appear to shrink as the boundary of the disc is approached: this is due to that shrinkage, and the true H^2 net has equal edges as well as equal angles.) Just as the elliptic patterns can be mapped into E^3 via projection onto the sphere (or any genus-zero surface), hyperbolic patterns can be projected from H^2 into E^3 via projection onto multi-handled hyperbolic surfaces embedded in E^3.

3. From 2D to (Euclidean) 3D space

To generate 3D *crystalline* patterns in E^3, we project onto crystalline hyperbolic surfaces embedded in E^3. This operation is delicate as H^2 cannot project directly into E^3 without some metric distortions (inducing variations of Gaussian curvature), in contrast to the possibility of an undistorted embedding of S^2 in E^3. The required distortions depend on the particular hyperbolic surface. For a variety of reasons, the simplest hyperbolic surfaces to adopt for this construction are the triply periodic minimal surfaces in E^3 (or IPMS). The attraction of IPMS as substrates for network reticulation (rather than other hyperbolic sponges) lies in the well-understood intrinsic 2D symmetry structure of IPMS, investigated already in detail to derive explicit parametrisation of IPMS [9]. To enable the projection, we construct an *atlas* of the IPMS, conformally equivalent on H^2 and the IPMS. The gridlines of the atlas are the in-surface mirror lines: these are the *intrinsic* mirrors lying *in* the IPMS (often distinct from the extrinsic 3D mirror planes, that are a function of the embedding of the IPMS in E^3)[2]. These gridlines give a map of the universal cover of the IPMS in H^2, by the following construction.

The symmetries of the map reveal the underlying hyperbolic orbifold. Its most compact form contains a single copy of the orbifold. The universal cover in H^2 consists of infinitely many copies of the orbifold, generated by repeated reflections in all (2D mirrors) boundary arcs. The orbifold pertaining to a particular IPMS is easy to determine from the symmetries of its Weierstrass parametrisation, in turn induced by the symmetries of the Gauss map of the IPMS. Indeed, the conformal structure of the IPMS at all points, except the isolated flat points, is identical to that of the Gauss map. The distortion of the surface conformal structure at flat points is a simple scaling of all angles, whose multiplicities depend on the order of branch points in the Gauss map (corresponding to flat points). For example, flat points, located on monkey saddles [1], lead to first order branch points in the Gauss map, and angles between arcs running through that flat point on the IPMS are multiplied by a factor of two in its Gauss map. We consider only arcs of reflection symmetry in the IPMS: (with the exception of the gyroid) these are plane lines of curvature or linear asymptotes in the surface. The Gauss map (whose domain can be taken to be the unit sphere, S^2), is thus a symmetric tiling of (possibly many covers of) S^2. A single asymmetric patch of the Gauss map, bounded by these mirror arcs, defines a single "kaleidoscopic" orbifold, whose Conway symbol is of the form $^*abc\ldots$ (It follows from differential geometry that a vertex of the S^2 orbifold whose Conway symbol entry exceeds four, or is uneven, is a flat point on the IPMS. Flat points can also be located on non-intersecting mirrors. We denote these sites by the redundant Conway symbol entry 1.) The analogous hyperbolic tiling that captures the conformal structure of the IPMS is formed by a symmetry mutation [7] of the Gauss map orbifold from spherical space, S^2, to hyperbolic space, H^2. The mutation rule is simple: the angle between intersecting mirrors of the orbifold must be divided by $(b+1)$, where b is the order of the corresponding point on the IPMS (zero for points on negative Gaussian curvature, positive for flat points) [10]. The corresponding Conway symbol entries for the IPMS are therefore simple multiples of that of its Gauss map. For example, the asymmetric domain of the Gauss map of the P and D surfaces is a spherical triangle, with vertex angles $\pi/2, \pi/4, \pi/3$. The last vertex is a first order branch point, so the relevant orbifold for the universal covering of

[2] These lines are the symmetry arcs of reflection symmetry of the complex *Weierstrass product polynomial* used to explicitly parametrise the surface from the complex plane to E^3 (via the Weierstrass equations) [9]. They can be determined explicitly by symmetry mutating the orbifold of the Gauss map of the surface (defined on S^2, therefore an elliptic kaleidoscopic orbifold), and depend on the elliptic orbifold and the branch-point order of the Gauss map surrounding flat points of the IPMS.

Table 2
Orbifold symmetries for the regular three-periodic minimal surfaces. The surface orbifolds are simple "symmetry mutations" of the orbifold of the Gauss map of the surfaces and their characteristics are given by Eq. (2)

Surface	Branch points	Surface orbifold (S^2)	Surface orbifold (H^2)	Orbifold (Euler–Poincaré) characteristic	Sub-group order (relative to *246)
Cubic P, D, G	{1, 1, 1, 1, 1, 1, 1, 1}	*243	*246	$-\frac{1}{24}$	1
tP, tD	"	*2214	*2224	$-\frac{1}{8}$	3
CLP	"	*2124	*2224	$-\frac{1}{8}$	3
C(P)	{2, 1 . . .}	$*4\frac{4}{3}3$	*446	$-\frac{1}{6}$	4
H	"	*2213	*2226	$-\frac{1}{6}$	4
hCLP	"	*2123	*2226	$-\frac{1}{6}$	4
F-RD	{2, 1 . . .}	$*22\frac{4}{3}\frac{3}{2}$	*2243	$-\frac{5}{24}$	5
I-WP	{2, 2, 2, 2}	$*2\frac{4}{3}2\frac{4}{3}$	*2424	$-\frac{1}{4}$	6
oCLP	"	*22112	*22222	$-\frac{1}{4}$	6
oPb, oDb	"	*21221	*22222	$-\frac{1}{4}$	6
rPD	"	*31313	*6262	$-\frac{1}{3}$	8
C(D)	{4, 1 . . .}	$*24\frac{3}{5}3$	*2436	$-\frac{3}{8}$	9
oPa, oDa	"	*222 (internal first order flat point)	*222222	$-\frac{1}{2}$	12

the P and D surfaces is a tiling of identical hyperbolic triangles with vertex angles $\pi/2, \pi/4, \pi/6$. Asymmetric domains of the Gauss map and the universal cover are bounded by mirrors by construction, so the relevant orbifolds are *243 and *246 respectively. The respective costs are $c = 1/24$ and $c = -1/24$, consistent with their elliptic (S^2) and hyperbolic (H^2) characters. All the IPMS orbifolds considered here are necessarily kaleidoscopic. The relevant orbifolds for all the "regular" IPMS, whose Gauss maps are described explicitly elsewhere [9], are given in Table 2.

Just as the Euclidean plane can be projected onto the cylinder by gluing points separated by the circumferential collar on the cylinder wrapping, projection of the universal cover of the orbifold in H^2 to E^3 results in the IPMS topology.

We make a number of observations about these IPMS orbifolds. First, all the orbifolds display integral ratios of costs with respect to the most symmetric case, *246. (That order can be deduced from the ratios of the orbifold characteristics.) However, they are not all sub-groups of *246. The group–sub-group relations for the simpler IPMS (excluding the F-RD and C(D) surfaces) can be classified into three families, related to the *246 (cost, $c = -2/48$), *248 ($c = -3/48$) and *24(12) ($c = -4/48$) orbifolds. The group–sub-group relations for those surfaces are shown in Fig. 3.

Those group–sub-group relations between the IPMS' orbifolds are useful: they allow a single H^2 tiling that is commensurate with one of the IPMS orbifolds to be mapped onto tilings commensurate with other IPMS. The distortion path from one case to another follows the symmetry relations of Fig. 3. In that way, a multiplicity of 3D Euclidean nets—realized by projection onto different IPMS, can be generated from a single 2D net. The idea will be illustrated by example below.

The *geometry* of the universal covering of IPMS is not uniquely constrained by the orbifold, though its conformal structure is fixed, with the exception of triangular kaleidoscopic orbifolds (of form $*abc$). For example, the geometry of the *2226 orbifold tiling[3], relevant to the H surface, can be deduced from the equations governing hyperbolic polygons. We split the quadrilateral into a pair of triangles, with angles and edges defined in Fig. 4.

A standard equation from hyperbolic trigonometry can be applied to the pair of triangles [11], equating their edge d:

$$\frac{\cos(\alpha)\cos(\beta) + \cos(\pi/6)}{\sin(\alpha)\sin(\beta)} = \frac{\sin(\alpha)\sin(\beta)}{\cos(\alpha)\cos(\beta)} \tag{3}$$

leading to the single constraint:

$$\cos(\alpha) = \sqrt{\frac{1}{4} - \frac{13}{16}\cos^2(\beta)} - \frac{3}{4}\cos(\beta). \tag{4}$$

Thus, the geometry of the tiles of the universal cover of the H surface contains a single free parameter. This corresponds to the single free parameter in the H surface itself: the unit cell axial c/a ratio of the hexagonal IPMS (present also in the Gauss map). Indeed, hyperbolic polygons with n edges and fixed vertex angles (e.g., kaleidoscopic orbifolds with n numerical entries in their Conway symbol) exhibit

[3] For convenience, we call the tiling induced by the universal cover of a kaleidoscopic orbifold in H^2 the "orbifold tiling".

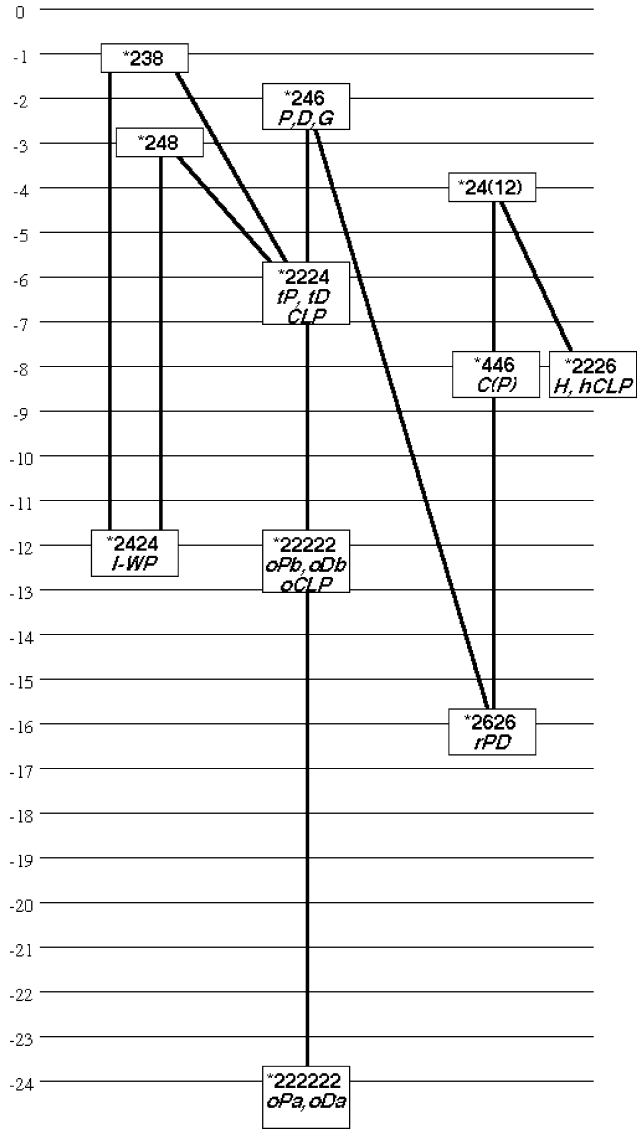

Fig. 3. Group–sub-group relations between the relevant orbifolds for simpler triply periodic minimal surfaces (IPMS, listed below the orbifold symbol) and related supergroup orbifolds. The cost of each orbifold locates the height of the orbifold entry (true cost equal to $-1/48$ times the values listed on the left) and the order of the sub-group relative to the group is equal to the ratio of costs.

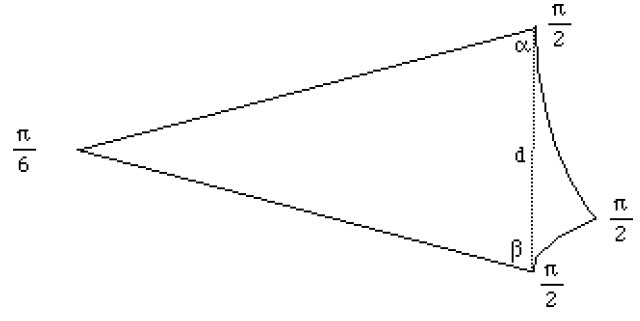

Fig. 4. A single tile of the universal covering of the H surface (the *2226 orbifold), a hyperbolic quadrilateral with vertex angles of $\pi/2, \pi/2, \pi/2$ and $\pi/6$. The dotted diagonal defines a pair of triangles, some of whose angles are marked within the tile.

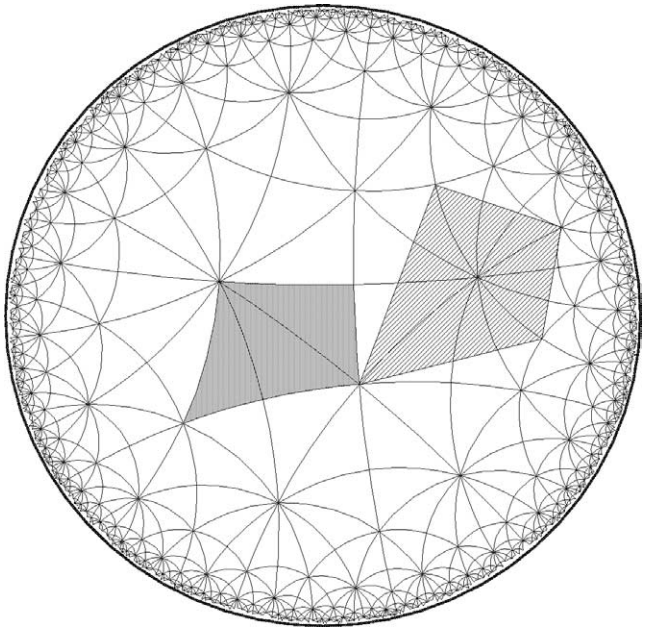

Fig. 5. The *246 tiling of H^2. Dotted (left) and hatched (right) domains are single orbifolds of order 3 and 6 sub-groups of *246: *2224 and *2424 respectively, relevant to the tP (and tD, tG) surfaces and the I-WP surface.

$(n-3)$ degrees of freedom. It follows then that the universal coverings of tetragonal and hexagonal IPMS have orbifold symbols with at least four numerical entries ($*abcd$) and orthorhombic cases have at least five numerical entries. Conversely, cubic IPMS generally lead to universal coverings of symmetry type $*abc$. Comparison with entries in Table 2 shows that this assertion fails for the cubic I-WP surface. In this case, however, the cubic symmetry of the surface is "accidental", as it is one member of the generic tetragonal class of IPMS [9].

It is worth commenting here on the connection between our orbifold approach and an earlier (profound) paper of Sadoc and Charvolin on IPMS crystallography [12]. They have discussed in some detail the gluing patterns for the P, D and G(yroid) IPMS with reference to the Platonic H^2 tilings (consisting of symmetrically identical faces, edges and vertices), denoted by their Schläfli symbols {6,4} and (its dual) {4,6}. Kaleidoscopic orbifolds have a natural association with a tiling, consisting of identical tiles. The infinite tiling is the universal cover of the kaleidoscopic orbifold in the relevant space (elliptic, Euclidean or hyperbolic), with a well-defined topology: each tile is a single copy of the orbifold and tile edges are the bounding mirrors of the (kaleidoscopic) orbifold. The H^2 tiling resulting from the universal cover of the *246 orbifold—germane to the P, D and G surfaces—consists of identical triangular tiles, with 4, 8 and 12 connected vertices in cyclic order about each tile (Fig. 5). The simplest regular polygonal tiles resulting in Platonic coverings of H^2 that are subgraphs of the full triangular tiling are the {6,4} and {4,6} tilings, discussed in detail by Sadoc and Charvolin. (The result is general: a $*24z$ orbifold yields $\{z, 4\}$ and $\{4, z\}$ as the maximal Platonic sub-

graph of the $^*24z$ universal covering.) The same construction gives {8,4} or {4,8} for the C(P) surface. Analogous tilings for other IPMS are not Platonic (the faces contain unequal edges). They have *topology* (5,4) or (4,5) for the oCLP, oPb and oDb surfaces; (6,4) or (4,6) for the CLP, tP, tD, oPa and oDa surfaces; (8,4) or (4,8) for the I-WP surface; (12,4) or (4,12) for the H and hCLP surfaces; (12,12) for the rPD surfaces.

4. 3D Euclidean (6.6.8) nets

The technique can now be applied to the (6.6.8) network mentioned in the Introduction. Consider first the most symmetric realisation of that network within its natural space, H^2: a decoration of the ^{*238} orbifold with a single (half) vertex (on an edge), inducing equivalent vertices (Figs. 1b, 2). ^{*238} (cost, $c = -1/48$) is a supergroup of order 12 of the ^{*2424} group ($c = -1/4$), characteristic of the I-WP surface (Fig. 3). This relation is evident in Fig. 2: the most symmetric form of the ^{*2424} orbifold contains twelve ^{*238} triangles. Superposition of the (6.6.8) network onto the universal covering of the I-WP surface can be done by inspection (Figs. 2, 6). The resulting tiling contains 6 vertices per ^{*2424} tile.

To form the (6.6.8) network in E^3, we use the diagram in Fig. 6, that represents the location of the (6.6.8) network on the I-WP surface "unglued" onto H^2. The 3D network results from regluing the universal cover in E^3, according to the gluing rules for the I-WP surface. The I-WP surface is a genus-four IPMS, so the surface can be unfolded into H^2 to give a (16,16) network [13], with eight gluing vectors required to refold the surface into the compact genus-four closed surface. To respect both the gluings and the translational symmetries of the I-WP surface, all eight identifications must be symmetries of the (6.6.8) pattern superimposed on the universal cover of ^{*2424}. (In formal language, the three-handled orbifold, "$\circ\ \circ\ \circ$" in Conway's notation, must be a subgroup of the group of the (6.6.8) tiling.) Clearly, the ^{*2424} group respects all eight identifications (^{*2424} is indeed a supergroup of the relevant $\circ\ \circ\ \circ$ orbifold). It follows that the distorted (6.6.8) superimposed on the ^{*2424} tiling can be projected onto the I-WP surface, as the symmetry of the pattern is itself ^{*2424}. The projection leads to a network containing (6.6.8) rings on the I-WP surface, and extra "collar" rings surrounding the ⟨111⟩ and ⟨100⟩ channels of the surface. The conventional cubic cell of the I-WP surface has Euler–Poincaré characteristic equal to -12 (twice genus four), containing 48 individual ^{*2424} tiles (cf. cost per orbifold, Table 2). The unit cell of the resulting E^3 (6.6.8) embedding thus contains $48 \times 6 = 288$ vertices.

Given a single Euclidean 3D embedding, via reticulation of the I-WP surface, we use next the group–sub-group relations of Fig. 3 to generate other (6.6.8) 3D Euclidean nets. Reticulations of the cubic P, D and Gyroid surfaces are feasible by (i) superposing the ^{*246} tiling on the ^{*2424} tiling, via the ^{*2224} tiling (the latter is an order 3 subgroup of the former, Fig. 3) and (ii) transposing the superposed (6.6.8) on ^{*2424} pattern to (6.6.8) on ^{*246}. The ^{*2224} pattern in H^2 is shown in Fig. 7. Unlike the ^{*2424} symmetry (6.6.8) tiling, this pattern does *not* respect all the intrinsic 2D symmetries of the cubic P, D, G tiling (^{*246}).

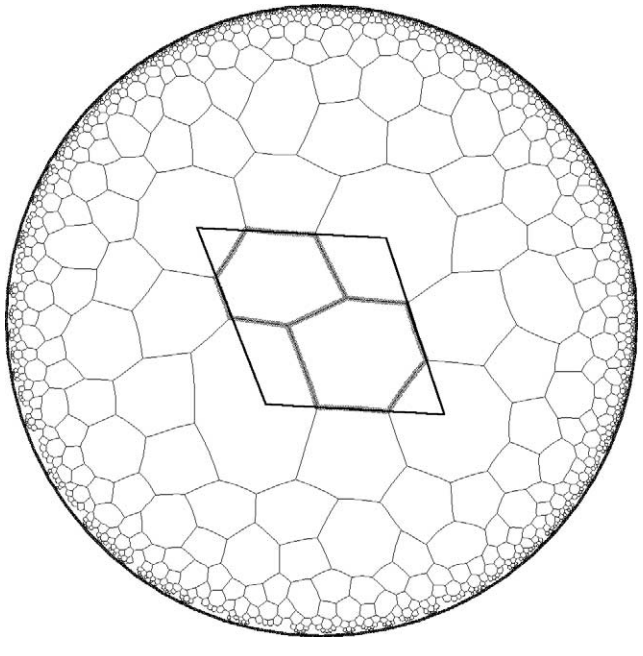

Fig. 6. (6.6.8) network in H^2 with ^{*2424} symmetry. A single orbifold is outlined and edges of the tiling within the orbifold are thickened.

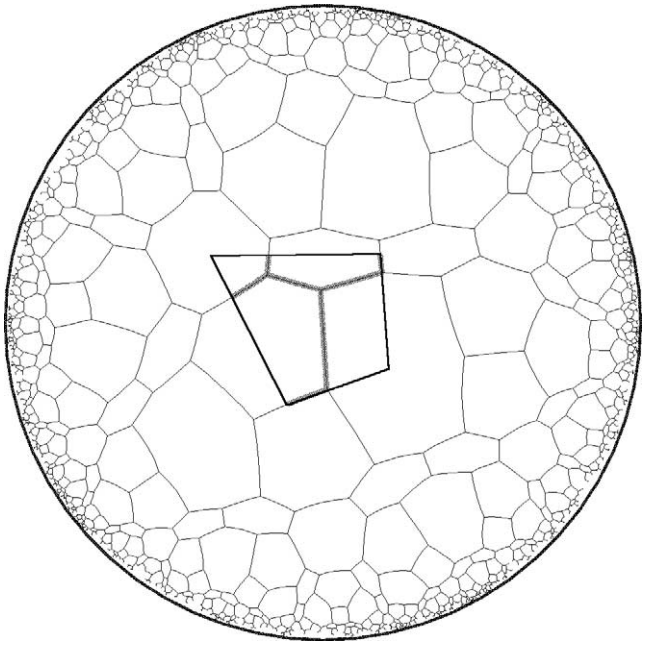

Fig. 7. Realisation of a (6.6.8) network in H^2 with ^{*2224} symmetry. A single orbifold is outlined and edges of the tiling within the orbifold are thickened.

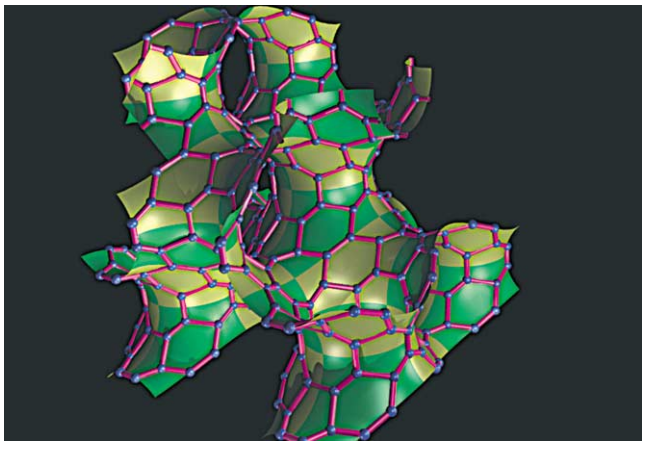

(a)

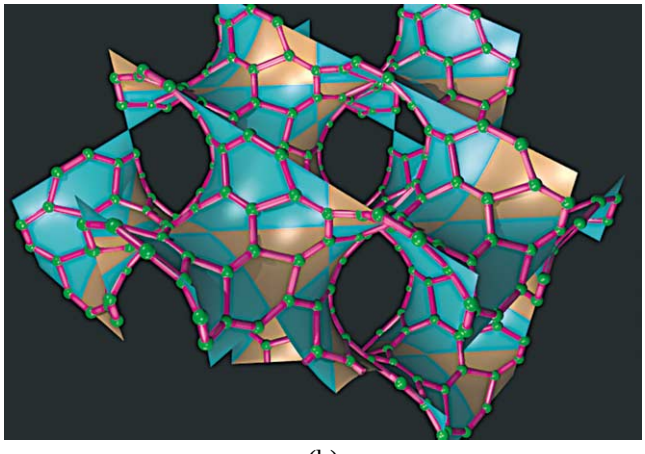

(b)

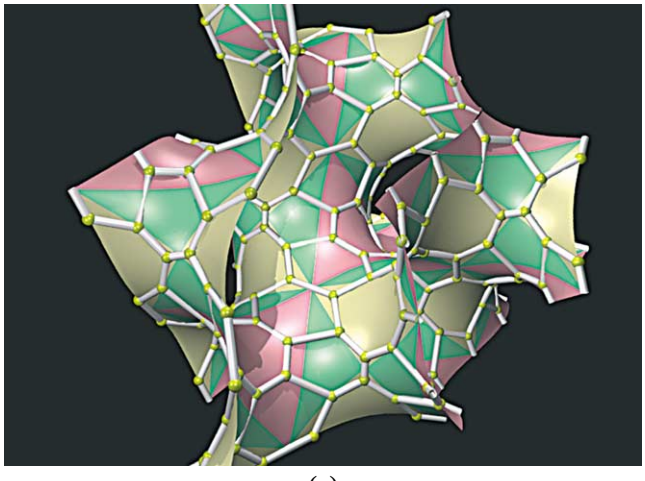

(c)

Fig. 8. Reticulations of the (a) P (b) D and (c) Gyroid minimal surfaces with the (6.6.8) network. The 3D Euclidean nets are projections of the hyperbolic pattern shown in Fig. 7 onto the P and D surfaces. For (the authors!) convenience, the surfaces are coloured to expose tilings of *22222 symmetry (a, b) and *336 symmetry (c).

The formation of (6.6.8) networks in E^3 by projection to the P, D and G surfaces is possible provided the P, D and G gluings are commensurate with the *2224 pattern. The gluings for these surfaces (discussed in [12]) are indeed translations of the (6.6.8) pattern, and the projection leads to P, D and G (6.6.8) networks in E^3 with three distinct topologies (including the collar rings) induced by the gluings.

The P, D and G surfaces are all genus-three surfaces, referred to their primitive oriented unit cells (of symmetry $Pm\underline{3}m$, $Fd\underline{3}m$ and $I4_132$, respectively). The conventional non-oriented unit cells (symmetries $Im\underline{3}m$, $Pn\underline{3}m$ and $Ia\underline{3}d$ resp.) thus have Euler characteristics equal to -4, -2 and -8. As they have three (6.6.8) vertices per *2224 orbifold (cost, $c = -1/8$), the P, D and G embeddings in E^3 of (6.6.8) have 96, 48 and 192 vertices per unit cell respectively. Images of the P and D embeddings are shown in Fig. 8.

5. Net relaxation in E^3

The projection of networks from H^2 to E^3 induces networks with curved geodesic edges, lying in the minimal surfaces. One final step remains: to "relax" the E^3 networks, forming geodesic edges in E^3 (straight lines) with maximal symmetry in E^3. This process generates a canonical representation of E^3 nets. We relax the net numerically, following modification of O'Keeffe's recipe [14]: the relaxed, maximally symmetric net is one with equal edges (normalized to one, for convenience) and maximal unit cell volume consistent with the network topology induced by the projection onto the sponges. The latter constraint is modified for our purposes: we seek instead to make all vertex angles as equal as possible, consistent with the imposition of equal edge lengths.

The numerical code we use runs as follows. The initial network geometry, consisting of a set of vertex positions in Cartesian space, (x_i, y_i, z_i), is obtained from the reticulation on the IPMS. That initial structure is then "relaxed" by motion under the influence of a vector force on each n-connected vertex. Those forces are calculated by the gradient of the (elastic) energy function, comprising edge length and vertex angle equalization components. We adopt the following form for the energy:

$$E = E_{\text{angle}} + E_{\text{length}} \tag{5}$$

with:

$$E_{\text{angle}} = \kappa_b \sum_{i,j,k=1}^{\frac{n(n-1)}{2}} (\pi - \theta_{ijk})^2 \tag{6}$$

and

$$E_{\text{length}} = \kappa_s \sum_{i,j=1}^{n} (d_{ij} - l)^2, \tag{7}$$

where κ_b, κ_s denote the elastic moduli for equalizing angles and edges respectively and l denotes the rest spring length. The indices i, j, k label the vertices. θ_{ijk} denotes the angle

Table 3
Crystallographic description of relaxed network configurations, with equal edges of unit length and maximal symmetry, for (6.6.8) nets projected onto the simpler IPMS. The net density is equal to the number of vertices per unit volume

Surface for projection	Space group symmetry (cell edges)	Vertices per unit cell (net density)	Vertex positions in asymmetric unit (crystallogr. coordinates)	Vertex angles
D	$P4_2/nnm$	48	(0,0.5,0.072)	130°, 115°, 115°
	($a = b = 5.32$ Å	(0.241)	(0.184,0.316,0.25)	120°, 120°, 120°
	$c = 7.04$ Å)		(0.294,0.426,0.044)	124°, 116°, 120°
			(0.147,0.412,0.132)	114°, 138°, 108°
P	$I4/mmm$	96	(0.138,0.436,0.209)	120°, 125°, 115°
	($a = b = 7.83$ Å	(0.223)	(0.213,0.436,0)	121°, 120°, 120°
	$c = 7.02$ Å)		(0.227,0.227,0.311)	118°, 121°, 121°
			(0.218,0.373,0.124)	143°, 113°, 105°
Gyroid	$I4_1/acd$	192	(0.008,0.062,0.623)	122°, 100°, 138°
	Non-standard setting:	(0.249)	(0.133,0.349,0.004)	142°, 101°, 117°
	$\underline{1}$ at (0.25,0.25,0.5)		(0.039,0.397,0.038)	142°, 108°, 110°
	($a = b = 8.97$ Å		(0.208,0.271,0.028)	106°, 123°, 131°
	$c = 9.57$ Å)		(0.143,0.428,0.334)	122°, 126°, 112°
			(0.384,0.027,0.126)	108°, 121°, 131°
I-WP	$Im\underline{3}m$	288	(0,0.209,0.406)	76°, 142°, 142°
	($a = b = c = 11.21$ Å)	(0.204)	(0,0.418,0.121)	118°, 118°, 124°
			(0.079,0.079,0.422)	107°, 107°, 146°
			(0.141,0.141,0.438)	111°, 138°, 111°
			(0.104,0.222,0.445)	78°, 143°, 139°

(centered on vertex i) subtended by the three (edge-linked) vertices i, j, k; of magnitude:

$$\theta_{ijk} = \arccos\left(\frac{d_{ij}^2 + d_{ik}^2 - d_{jk}^2}{2d_{ij}d_{ik}}\right),$$

where d_{ij} denotes the distance of the vector joining vertices i and j. That metric is dependent on the cell parameters (edges a, b and c and cell angles α, β, γ) as well as vertex positions:

$$d_{ij} = \begin{pmatrix} (x_j - x_i)^2a^2 + (y_j - y_i)^2b^2 + (z_j - z_i)^2c^2 \\ +2(x_j - x_i)(y_j - y_i)ab\cos(\gamma) \\ +2(y_j - y_i)(z_j - z_i)bc\cos(\alpha) \\ +2(z_j - z_i)(x_j - x_i)ac\cos(\beta) \end{pmatrix}^{\frac{1}{2}}.$$

Periodic boundary conditions are imposed on a single unit cell of the network, to mimic the crystal framework. The relaxation is achieved by allowing deformation of the unit cell shape as well as vertex sites within the cell. The energy therefore depends on $x_i, y_i, z_i, a, b, c, \alpha, \beta, \gamma$.

The force acting on each n-connected vertex is the gradient of E respect to x_i, y_i, z_i:

$$F_{x_i} = -\frac{\mathrm{d}E}{\mathrm{d}x_i}; \quad F_{y_i} = -\frac{\mathrm{d}E}{\mathrm{d}y_i}; \quad F_{z_i} = -\frac{\mathrm{d}E}{\mathrm{d}z_i}.$$

In order to minimize the energy, the position of the vertices changes by an amount proportional to these forces:

$$\mathrm{d}x_i \propto F_{x_i}; \quad \mathrm{d}y_i \propto F_{y_i}; \quad \mathrm{d}z_i \propto F_{z_i}.$$

The "forces" acting to deform the unit cell are calculated from Eqs. (5)–(7) and:

$$F_a = -\frac{\mathrm{d}E}{\mathrm{d}a}; \quad F_b = -\frac{\mathrm{d}E}{\mathrm{d}b}; \quad F_c = -\frac{\mathrm{d}E}{\mathrm{d}c},$$
$$F_\alpha = -\frac{\mathrm{d}E}{\mathrm{d}\alpha}; \quad F_\beta = -\frac{\mathrm{d}E}{\mathrm{d}\beta}; \quad F_\gamma = -\frac{\mathrm{d}E}{\mathrm{d}\gamma},$$

which give

$$\mathrm{d}a \propto F_a; \quad \mathrm{d}b \propto F_b; \quad \mathrm{d}c \propto F_c$$

and

$$\mathrm{d}\alpha \propto F_\alpha; \quad \mathrm{d}\beta \propto F_\beta; \quad \mathrm{d}\gamma \propto F_\gamma.$$

In practice, the magnitudes of the elastic moduli are tuned to ensure convergence to a final configuration with all edges of equal length (l) and angles as nearly equal as possible.

Canonical, maximally symmetric, network geometries for the (6.6.8) examples induced by projection onto the I-WP, P, D and G IPMS described above are listed in Table 3. We note that the latter three projections induce tetragonal networks, consistent with the ^{*2224} symmetry (that of tetragonal IPMS, cf. Table 2) of their hyperbolic counterparts (Fig. 6). The G network is chiral, induced by the chiral projection of H^2 to E^3 forming the G surface. The projections onto IPMS induce channels in the E^3 embeddings; these are surrounded by "collar rings" that surround the channels. The collar rings consist of 18 vertices for the I-WP network, 14- and 20-rings for the P network and 18-rings for the D and G networks (Fig. 9).

The relaxed structures are of variable "regularity", compared to an ideal regular three-connected net with equal edge lengths and all vertex angles equal to $2\pi/3$[4]. The variations in vertex angle are due to three effects: (i) the inherent irregularity in the H^2 universal cover, (ii) distortions induced by the projection onto IPMS and (ii) angle variations induced

[4] The (6.6.8) net cannot be realised as a regular net, even in H^2. See Note added in proof at end of article.

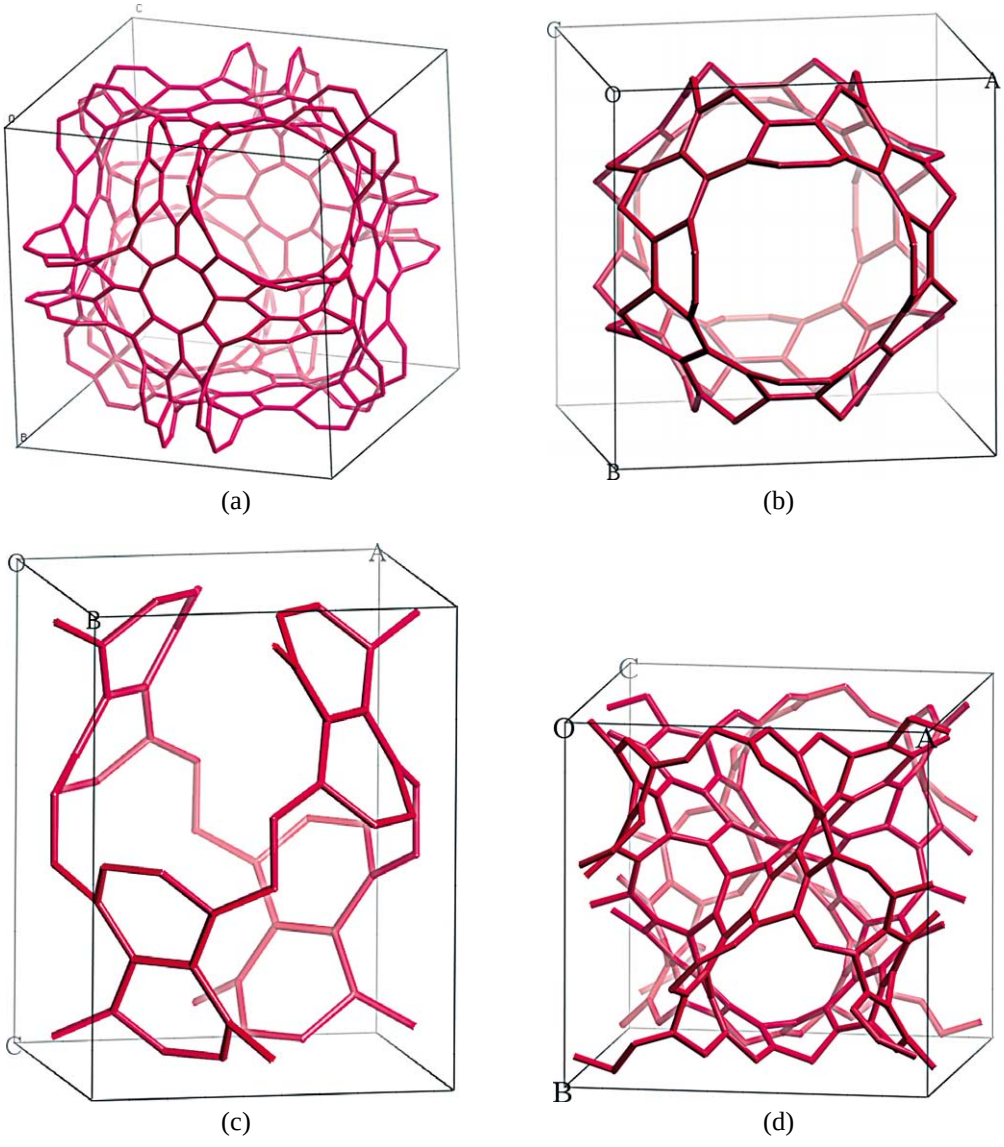

Fig. 9. Relaxed (6.8.8) nets formed by reticulations of IPMS. (a) The (cubic) I-WP surface reticulation, (b) the (tetragonal) P reticulation, (c) the (tetragonal) D reticulation and (d) the (tetragonal) Gyroid reticulation. (Crystallographic descriptions are listed in Table 3.)

by the relaxation process in E^3. Note first that the most symmetric (6.6.8) net in H^2 is itself irregular. The lower symmetry *2224 and *2424 (6.6.8) embeddings are less regular still. The second and third sources of geometrical distortion, the E^3 projection and subsequent relaxation process, are dependent on the variations in Gaussian curvature in the IPMS relative to H^2 and the surface embedding in E^3. The P/D/G family of IPMS are more uniformly curved than the I-WP surface. That effect is likely to be the principal cause of the extreme irregularity of the I-WP reticulation compared with the others. The I-WP reticulation is unlikely to be useful for carbon frameworks, due to the wide variability of vertex angles. The P, D and G reticulations are more regular and are perhaps reasonable candidate structures for novel carbon frameworks.

A strong correlation between the network topology and the geometric density of the relaxed configuration has been noted elsewhere for a range of nets, including theoretical carbon frameworks and zeolites [15]. The theoretical density of a $\{p, q\}$ network, r, defined to be the number of vertices per unit volume (for edges of unit length), can be expressed in terms of the two-dimensional surface reticulation and ring sizes as follows:

$$r = \left(\frac{H}{\Omega^{3/2}}\right)\left(\frac{q + (1 - q/2)}{p}\right). \tag{8}$$

The (6.6.8) frameworks have connectivity, $q = 3$ and average ring size,

$$p = \frac{3}{1/6 + 1/6 + 1/8}.$$

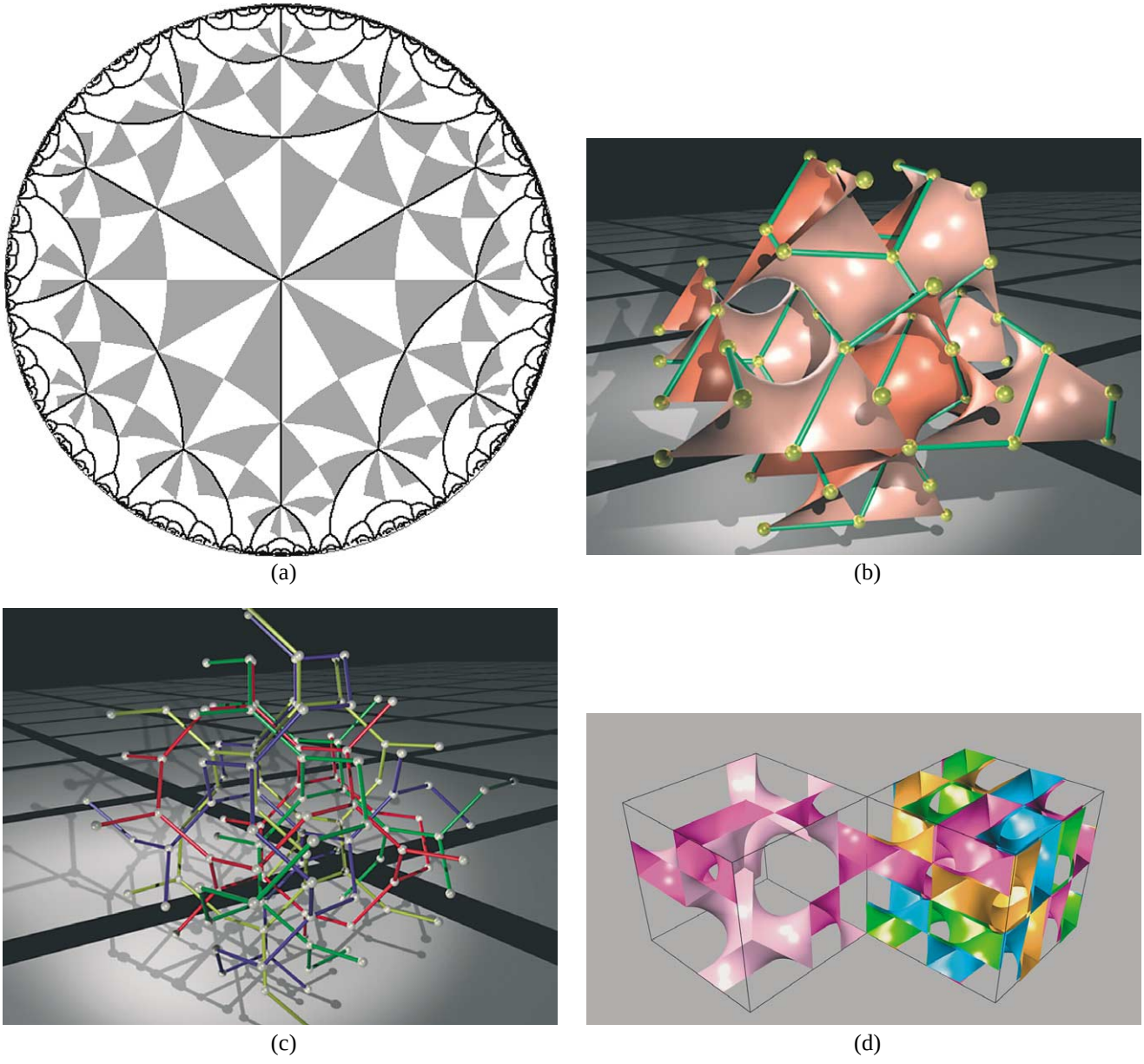

Fig. 10. (a) A dense packing of 3-connected regular trees in H^2 of edge length arcosh(3), commensurate with the *246 orbifold tiling (alternately coloured tiles). (b) Projection of (a) onto the D surface. (c) The pattern of edges in (c): a quartet of identical, interwoven, chiral Y* nets. (d) The quadracontinuous minimal surface whose channels are those of (c). (For clarity a pair of closely separated parallel surfaces, displaced to both sides of the minimal surface, is shown.) Each domain is coloured distinctly, one domain is extended into an adjacent unit cell.

The homogeneity index, H is close to its ideal value of 3/4 for IPMS, equal to 0.7776, 0.7498, 0.7425 and 0.7163 for the G, D, I-WP and P surfaces respectively. The area per vertex of the surface reticulation can be estimated from the Euclidean equation [15]:

$$\Omega \approx \frac{q}{4}\tan\left(\frac{\pi}{q}\right).$$

Substitution of these values into Eq. (8) gives the estimates:

$$r_D = 0.236; \quad r_P = 0.225; \quad r_G = 0.241; \quad r_{\text{I-WP}} = 0.233.$$

The agreement between these estimates and actual values (Table 3) is impressive.

6. Generalisations

Sten Andersson's 1983 review [1] contains the following lines: "*can a minimal surface divide space into three or more interpenetrating subvolumes? This I do not know*". Only now, two decades later, can we respond: "Yes, a number

of solutions exist". The projection algorithm can be used to generate examples [10,16].

They are particularly beautiful, as they result from projections of *trees* (with no rings) from H^2 to E^3. In contrast to their Euclidean counterparts, regular trees, with (an infinity of) identical edges and vertices and free of self-intersections, are found in H^2. Indeed, identical trees can be close-packed in H^2, to yield a dense forest [10] (Fig. 10a). If the edge length of the trees is tuned to be commensurate with an IPMS orbifold, the forests can be projected onto IPMS (Fig. 10b), and thereby projected from H^2 to E^3. For example, a dense forest of three-connected trees with edges equal to arcosh(3) is a sub-group of ^{*246}. Projection onto the D surface is therefore allowed. The resulting reticulations generally consist of multiple disjoint interwoven networks, analogous to the pair of interwoven nets defining the channels of "bicontinuous" IPMS (Fig. 10c).

These projected forests can be considered as channel systems of "multicontinuous" space partitions. One particularly pretty example is the quadracontinuous, chiral surface, whose faces are minimal surfaces, edges are common to three faces with dihedral angles of $2\pi/3$ and vertices link four incident edges, whose angles are tetrahedral (Fig. 9d). The multicontinuous partition fulfills Plateau's rules for a stable froth; it is a *chiral foam*, containing four infinite bubbles. Moreover, this new spatial partition bears a fascinating relation to the gyroid IPMS. Twenty years ago, Sten, Kåre Larsson and one of us (STH) spent an exciting few months generating the gyroid. Sten realized the importance of that minimal surface in chemical systems, from the solid state (zeolites and mesoporous materials), and Kåre recognized its relevance to soft materials (liquid crystals and cell membranes). The channel system of each bubble in the triply periodic quadracontinuous minimal surface is precisely that of a single channel of the gyroid. The gyroid IPMS contains two interwoven right- and left-handed Y^* labyrinths (Y^{*+} and Y^{*-}), the new quadracontinuous example contains four interwoven Y^{*+} (or four Y^{*-}) labyrinths. The new quadracontinuous minimal surface is but one example of structures that partition E^3 into identical cells (open or closed). Other examples are conventional convex polyhedra and curved surfaces, including IPMS, both employed to great advantage by Sten and colleagues to understand crystal structures over the years. Can we find this new example in Nature too?

Note added in proof

While the ^{*236} decoration can be arranged with equal edge lengths so that all vertex angles are equal, and the resulting {6,3} network is regular, regular tilings are impossible for (6.6.n), where n exceeds six. Standard formulae from hyperbolic trigonometry [11] lead to the following relation between the edges a and b and the angle α (cf. Fig. 1b):

$$\frac{a}{b} = \frac{\operatorname{arcosh}\left(\frac{\cos(\pi/3)}{\sin(\pi/n)}\right) - \operatorname{arsinh}\left(\frac{((\frac{\cos(\pi/n)}{\sin(\pi/\alpha)})^2+1)^{1/2}}{\sin(\pi/n)}\right)}{\operatorname{arcosh}\left(\frac{\cos(\pi/n)}{\sin(\pi/\alpha)}\right)}. \tag{3}$$

Imposing the constraint of equal edge lengths implies the angle $\alpha = 2.792$ for the (6.6.8) tiling, leading to vertex angles of 115.53°, 115.53° and 128.94°. (It is a curious fact that two of the vertex angles for generic hyperbolic (6.6.n) tilings approach tetrahedral vertex angles as n increases (the three vertex angles for the (6.6.∞) tiling are $\arccos(-\frac{1}{3})$, $\arccos(-\frac{1}{3})$, $2\pi - 2\arccos(-\frac{1}{3})$.)

References

[1] S. Andersson, Angew. Chem. Int. Ed. Engl. 22 (1983) 69.
[2] M. O'Keeffe, G.B. Adams, O.F. Sankey, Phys. Rev. Lett. 68 (1992) 2325.
[3] H. Terrones, A.L. Mackay, Chem. Phys. Lett. 207 (1993) 45.
[4] J. Montesinos, Classical tessellations and Three-Manifolds, Springer-Verlag, Berlin, 1987.
[5] J.H. Conway, Groups, Combinatorics and Geometry, in: Lond. Math. Soc. Lecture Note Series, Vol. 47, 1992, p. 438.
[6] H.S.M. Coxeter, Regular Polytopes, Dover, New York, 1973.
[7] D. Huson, Two-dimensional symmetry mutation, available at www.mathematik.uni-bielefeld.de/~huson/papers.html.
[8] A. Ramsay, R.D. Richtmayer, Introduction to Hyperbolic Geometry, Springer-Verlag, New York, 1995, p. 210.
[9] A. Fogden, S.T. Hyde, Acta Crystallogr. A 48 (1992) 575.
[10] S.T. Hyde, C. Oguey, Eur. Phys. J. B 16 (2000) 613.
[11] J. Ratcliffe, Foundations of Hyperbolic Manifolds, Springer-Verlag, Berlin, 1994.
[12] J.-F. Sadoc, J. Charvolin, Acta Crystallogr. A 45 (1989) 10.
[13] D. Hilbert, S. Cohn-Vossen, Geometry and the Imagination, Chelsea Publ. Co., New York, 1952.
[14] M. O'Keeffe, Z. Kristallogr. 196 (1991) 21.
[15] S.T. Hyde, Acta Crystallogr. A 50 (1994) 753.
[16] S.T. Hyde, S. Ramsden, in: D. Bonchev, D.H. Rouvray (Eds.), Chemical Topology. Applications and Techniques, Gordon and Breach Science Publ., Amsterdam, 2000.